Strong Correlations Enhanced by Charge Ordering in Highly Doped Cobaltates

Oleg E. Peil, Antoine Georges, and Frank Lechermann

Strong correlations enhanced by charge-ordering in highly doped cobaltates

Oleg E. Peil,[1] Antoine Georges,[2, 3, 4] and Frank Lechermann[1]

[1] *I. Institut für Theoretische Physik, Universität Hamburg, D-20355 Hamburg, Germany*
[2] *Centre de Physique Théorique, École Polytechnique, CNRS, 91128 Palaiseau Cedex, France*
[3] *Collège de France, 11 place Marcelin Berthelot, 75005 Paris, France*
[4] *DPMC, Université de Genève, 24 Quai Ernest Ansermet, 1211 Genève 4, Suisse*

We present an explanation for the puzzling spectral and transport properties of layered cobaltates close to the band-insulator limit, which relies on the key effect of charge ordering. Blocking a significant fraction of the lattice sites deeply modifies the electronic structure in a way that is shown to be quantitatively consistent with photoemission experiments. It also makes the system highly sensitive to interactions (especially to intersite ones), hence accounting for the strong correlations effects observed in this regime, such as the high effective mass and quasiparticle scattering rate. These conclusions are supported by a theoretical study of an extended Hubbard model with a realistic band structure on an effective kagomé lattice.

The layered cobaltate metals are famous for their remarkable electronic properties [1], ranging from a large thermoelectric response [2], charge ordering [3, 4] and puzzling magnetic behavior, to superconductivity when intercalated with water [5]. Due to the universality of the physical properties throughout the cobaltate family, it is believed that most of these properties have their roots in the electronic structure of the CoO_2 layers. Those are formed of edge-sharing octahedra, with the Co ions forming a triangular lattice. Either alkali(-earth) metals (Na, Li, Ca etc., as in Na_xCoO_2), or more complex building blocks (e.g. rocksalt BiO or SrO planes in misfit cobaltates [6]) separate the layers and serve as electron donors. Varying the composition of the intercalated compounds controls the doping $x \in [0, 1]$, resulting in a nominal $Co^{(4-x)+}$ ($3d^{5+x}$) valence in the low-spin configuration within the t_{2g} manifold. The latter is split by the local trigonal symmetry into one a_{1g} and two e'_g states. Strong Coulomb interactions have been documented [7] to occur within this orbital subspace.

Remarkably, most of the signatures of strong correlations in cobaltates, such as specific-heat enhancement [8], band narrowing [7, 9–11] or strong electron-electron scattering [12] are observed in the high-doping region $x \in [1/2, 1]$ close to the band-insulating limit ($x = 1$). Besides intriguing magnetic behavior, charge disproportionation as well as intricate Na ordering [3, 4, 13–15] are prominent features in this part of the phase diagram for sodium cobaltate. In $Na_{3/4}CoO_2$ clear evidences of separation of Co-ions into non-magnetic Co^{3+}-ions and magnetic ions with a mixed valence are present [16, 17]. Importantly, this charge segregation is not restricted to selected dopings, but the concentration of Co^{3+}-ions is experimentally verified to steadily increase with doping starting from $x = 1/2$ [18]. Recently, the nuclear-magnetic-resonance (NMR) experiments of Alloul et al. [4] revealed for $x = 2/3$ a charge-ordering pattern of cobalt ions with valency close to Co^{3+}, with the remaining $Co^{3.44+}$ ions forming an effective kagomé lattice (EKL). The rather complex three-dimensional unit cell has common features revealed within a previous theoretical electronic-structure study [15] and links the charge order to a tailored order of the Na ions. As far as it concerns the electron-lattice coupling, it is, however, still a matter of debate whether the sodium ordering or intrinsic correlation effects within the CoO_2 layers are dominant in inducing the charge ordering in these systems.

In this Letter, we demonstrate that many puzzling physical properties of cobaltates at high doping may be understood within a picture of correlated itinerant electrons moving in a charge-ordered background. Charge-disproportionation patterns of Co^{3+}-ions with well-localized electrons are formed, restricting the remaining carrier dynamics to an effective lattice with an open structure. Such a system is shown to be highly sensitive to correlations, both because of a prominent van-Hove singularity close to $x = 0.7$ (owing to higher-order hopping terms) and due to the strong effect of intersite Coulomb interactions in line with the high susceptibility to charge-density wave (CDW) formation near $x = 3/4$.

To substantiate this view we consider a particular realization of charge ordering, namely the EKL detected at $x = 2/3$ for Na_xCoO_2 up to room temperature [4]. Whereas the charge-ordering at $x = 1/2$ seems unique to that stoichiometry, $x = 2/3$ also marks the onset of Curie-Weiss behaviour and enhanced spin fluctuations, leading eventually to in-plane ferromagnetic order for $3/4 < x < 0.9$. Furthermore, it is a commensurate doping for CDW instabilities on the triangular lattice (as studied e.g. in Ref. [19] within the Gutzwiller approach). Importantly, a recent calculation of the charge susceptibility in sodium cobaltate for the Hubbard model shows tendencies to the kagomé instability at large x even when disregarding the specific sodium distribution [20]. Note however that disordered donor configurations can by themselves enhance the correlation effects in the CoO_2 layers [21] and also magneto-polaronic excitations were suggested to play a role in this context [22].

In what follows, we address the spectral and transport properties of cobaltates stemming from a charge-order-
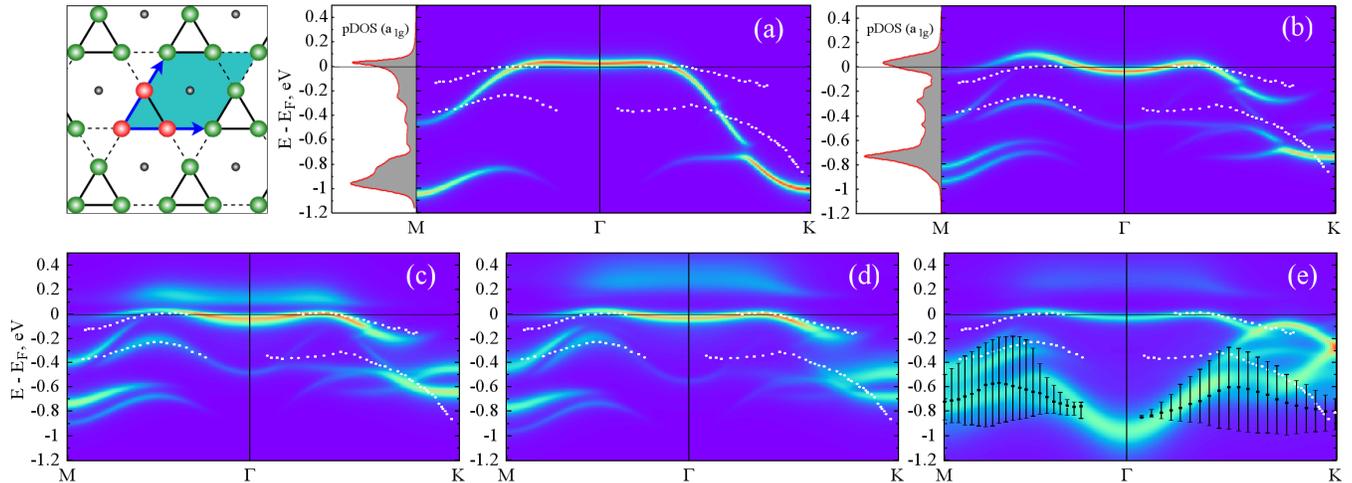
FIG. 1. (color online) Top left panel: Sketch of the EKL, with blocked sites depicted by small spheres and the shaded region representing the unit cell. Panels (a-e): Unfolded spectral functions $A(\mathbf{k}, \omega)$ (according to Eq. (3)) projected onto a_{1g} orbitals (a-d) and onto both a_{1g} and the two e'_g orbitals (e) for $Na_{2/3}CoO_2$ ($T = 115K$). Top panels (a-b): results for ($U = V = 0$) on the triangular lattice (a), and on the kagomé lattice (b), with the side-panels displaying the corresponding k-integrated spectral function. Bottom panels (c-e): results obtained within CDMFT for $U = 5$ eV, $V = 0$ (c) and for $U = 5$ eV, $V = 0.3$ eV (d), (e). The white dotted lines in (a-d) represent the QP peak and HE hump extracted from the ARPES data in Refs. 9 and 10. In (e) the black dotted lines correspond to the locations of the energy-distribution-curve (EDC) maxima of the spectral intensity seen at high energies in the bare ARPES data of Refs.9 and 10 (with black bars showing the approximate width of the feature). The quasiparticle and HE hump dotted lines in (e) are the same as in the other panels.

induced EKL (see Fig. 1), where the sodium and oxygen degrees of freedom are integrated out. The EKL doping y is related to the physical doping x on the triangular lattice by $y = (4x - 1)/3$. The full t_{2g} manifold is included in the modelling, however explicit two-particle interactions are only treated for a_{1g}, since it is known that the e'_g bands lie below the Fermi level ε_F for the high-doping regime. Our realistic model on the EKL is defined by an extended Hubbard Hamiltonian $\hat{\mathcal{H}} = \hat{H}_0 + \hat{H}_{int}$ with

$$\hat{H}_0 = - \sum_{\sigma \langle ij \rangle \alpha \beta} t_{ij}^{\alpha\beta} \hat{c}_{\sigma i}^{\alpha\dagger} \hat{c}_{\sigma j}^{\beta} + \Delta \sum_{\sigma i} \hat{n}_{\sigma i}^1 , \quad (1)$$

$$\hat{H}_{int} = U \sum_i \hat{n}_{\uparrow i}^1 \hat{n}_{\downarrow i}^1 + V \sum_{\langle ij \rangle} \hat{n}_i^1 \hat{n}_j^1 , \quad (2)$$

where the hopping matrix $t_{ij}^{\alpha\beta}$ is parametrized up to the third nearest-neighbor (NN) from the band structure of $Na_x CoO_2$ within the local-density approximation. Orbital indices are $\alpha = 1$ for a_{1g} and $\alpha = 2, 3$ for e'_{g1}, e'_{g2}. The parameter Δ fixes the a_{1g}-e'_g renormalized crystal-field splitting. We choose $U = 5$ eV in line with experimental and theoretical determinations [7, 23] and varied the NN intersite Coulomb interaction V up to 0.3 eV. Decreasing U down to 3.5 eV provided no significant variation of the results.

The band structure of the non-interacting realistic model consists of nine bands inside the Brillouin zone (BZ) of the EKL. To connect to the results of angle-resolved photoemission (ARPES) experiments we repre-

sent the computed k-resolved spectral function in the BZ of the underlying triangular lattice. This can be achieved, following the method of Ref. 24, by "unfolding" the nine bands in the supercell kagomé-lattice BZ (SBZ) to the three bands in the normal BZ (NBZ) of the triangular lattice. The states $|\mathbf{K}\alpha\rangle$ defined within the SBZ are projected onto the states $|\mathbf{k}\alpha\rangle$ defined in the NBZ, so that the spectral function projected on orbital α reads:

$$A_\alpha(\mathbf{k}, \omega) = -\frac{1}{\pi} \sum_{\mathbf{K}ll'} \langle \mathbf{k}\alpha | \mathbf{K}l \rangle \operatorname{Im} G_{ll'}(\mathbf{K}, \omega) \langle \mathbf{K}l' | \mathbf{k}\alpha \rangle , \quad (3)$$

where $\mathbf{K} \in$ SBZ and $\mathbf{k} \in$ NBZ. The lattice Green's function, $G_{ll'}(\mathbf{K}, \omega) = [(\omega + \mu)\delta_{ll'} - H_{0,ll'}(\mathbf{K}) - \Sigma_{ll'}(\mathbf{K}, \omega)]^{-1}$ is written in the basis $|l\rangle \equiv |i, \alpha\rangle$, where i runs over the three atoms of the kagomé-lattice unit cell.

To examine the spectral properties, we project $A(\mathbf{K}, \omega)$ onto the a_{1g} and e'_g orbitals and unfold the EKL bands into the NBZ. The obtained spectral functions are compared to the ARPES data of Nicolaou *et al.* for $x = 0.7$ [9, 10]. Although those data were obtained for misfit cobaltates (BiO and BaO planes), at present stage the spectra obtained for sodium cobaltates are qualitatively very similar (see e.g. [25], [11]). The analysis of the polarization-dependence of the ARPES spectra performed by the authors of Ref. [9, 10] led them to identify two a_{1g}-like features: a low-energy quasiparticle (QP) peak close to ε_F, and a high-energy (HE) hump around

-0.4 eV, both shown as dotted lines on Fig. 1.

Already for $U = V = 0$ the theoretical spectral function of the EKL is found to be in much better agreement with experiment than that of the original triangular structure without charge order, as shown in Fig. 1a, b. The HE hump identified experimentally, and completely absent in the triangular-lattice model, matches quite well with the HE feature around -0.4 eV in the EKL model. This HE feature originates here from a_{1g}-e'_g hybridizations (cf. Fig. 1e where the full t_{2g} projection is shown) induced by the loss of the original full triangular symmetry. It is thus essential to keep the e'_g states in the model to reproduce the spectral structure in this energy range around the Γ-point. In contrast, in Ref. 9 and 10 the HE feature was interpreted as an incoherent excitation with a_{1g} character of unknown type. However, it should be noted that the full local triangular symmetry with equivalent Co sites together with a compensation between the spectra of the two e'_g orbitals were assumed in the analysis of Ref. 9 and 10 in order to extract an a_{1g} signal. Since triangular symmetry is broken in the charge-ordered phase, refinements in the polarization-dependent analysis of the ARPES data may be required.

The full interacting model is solved by dynamical mean-field theory (DMFT) and its cellular-cluster extension (CDMFT) [26]. A continuous-time quantum Monte Carlo solver within the hybridization-expansion approach [27] is used, in the implementation by Parcollet and Ferrero [28]. The cluster impurity model is defined in terms of a natural basis of molecular orbitals via $|d_1\rangle = (-2\,|1\rangle + |2\rangle + |3\rangle)/\sqrt{6}$, $|d_2\rangle = (|2\rangle - |3\rangle)/\sqrt{2}$, $|u\rangle = (|1\rangle + |2\rangle + |3\rangle)/\sqrt{3}$, where $|i\rangle$, $i = 1, 2, 3$ denote states corresponding to the basis atoms of the kagomé-lattice unit cell. In this representation the impurity self-energy matrix is diagonal with elements $(\Sigma_d, \Sigma_d, \Sigma_u) = (\Sigma_0 - \Sigma_1, \Sigma_0 - \Sigma_1, \Sigma_0 + 2\Sigma_1)$, where Σ_0, Σ_1 are the on-site and intersite self-energies, respectively.

In terms of spectral properties, the on-site U-term alone ($V = 0$) already yields a significant renormalization of the QP band: its bandwidth is reduced by a factor $Z \simeq 0.4$ (compare panels (b) and (c) in Fig.1). Spectral-weight transfer takes place to an incoherent upper Hubbard band above ε_F (Fig. 1c). But the strongest effect of U actually manifests itself in a high value of the inverse QP lifetime $\Gamma \equiv -Z \operatorname{Im} \Sigma(i0^+)$. Figure 2 displays the dimensionless ratio $\Gamma/k_B T$ vs. T evaluated in DMFT. Remarkably, this ratio is significantly larger than unity for almost all temperatures and doping studied. Thus, long-lived coherent QPs only exist at very low T, due to electron-electron scattering. Extrapolation of our numerical results suggest that the coherent regime ($\Gamma/k_B T < 1$) would be reached only for $T \lesssim 20$K at $x = 2/3$, and the true Fermi-liquid behaviour ($\Gamma/k_B T \propto T$) at an even lower temperature scale. This is qualitatively consistent with the large values of the resistivity reported in this
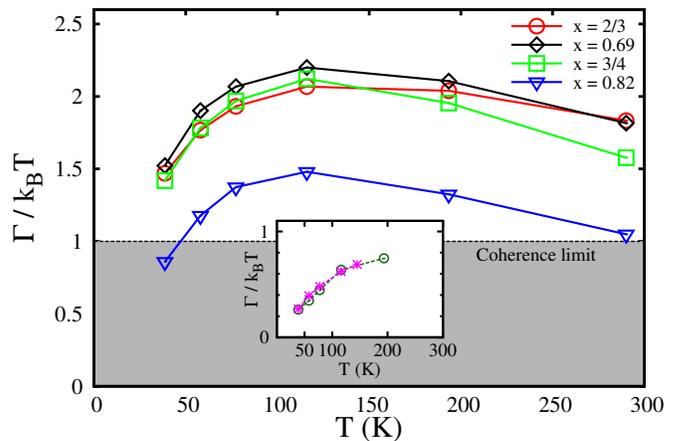
FIG. 2. (color online) Temperature-dependence of $\Gamma/k_B T$, with Γ the inverse QP lifetime for the kagomé cobaltate model with on-site Coulomb interaction U ($V = 0$) for different x. Inset: $\Gamma/k_B T$ for the triangular cobaltate model including distant hoppings at $x = 3/4$ (green, circles) and for the kagomé lattice with only NN hoppings at $x = 2/3$ (magenta, stars).

doping regime (e.g. $\rho \sim 300\mu\Omega$cm for $\mathrm{Na_{0.71}CoO_2}$ at $T = 100$K [1]), as well as with the huge scattering rate at low T [12] and the low value of the saturation temperature of the susceptibility [29]. The value of Γ is largest for $x \simeq 0.69$, which is approximately the doping at which the van-Hove singularity lies at the Fermi level (see side-panel of Fig. 1b). Notably, only the EKL model with realistic hoppings shows this characteristics, while sole NN hoppings (having no flat dispersions near ε_F at large x for $t < 0$) lead to a low scattering rate (inset of Fig. 2). The behavior of the system is strongly modified when the intersite interaction, $V > 0$, is taken into account. Figure 3 displays the QP weight Z_u from CDMFT for the 'symmetric' molecular orbital of the EKL as a function of x for increasing V. For $x = 2/3$, V has only moderate effect, although it does reduce Z by a factor of two, bringing it close to the experimentally observed mass enhancement ($m^*/m_{\mathrm{LDA}} \simeq 4$). Some improvement in the comparison to ARPES at this doping is also found (Fig. 1d,e). In contrast, close to $x = 3/4$, the system is highly sensitive to V. Indeed, this doping level corresponds to the commensurate doping $y = 2/3$ on the EKL, at which a non-zero V can induce a CDW instability towards an insulating state. We find this to happen at a rather small value of $V_c = 0.1$ eV (inset of Fig. 3). This renders it possible that a very strongly correlated metallic state (with a small QP weight renormalized by charge fluctuations) found close to $x = 3/4$, is best described as a weakly doped CDW insulator. It is also worth mentioning that $x = 3/4$ is the doping for the onset of magnetic ordering, and that transport anomalies were observed at this doping [30].

Note that previous works already showed the impor-
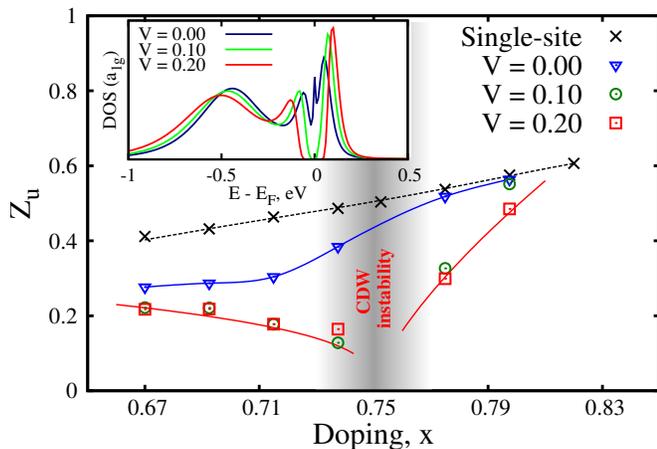
FIG. 3. (color online) Doping-dependence of Z for the symmetric molecular orbital $|u\rangle$ of the kagomé cobaltate model at $T = 39K$. Crosses: single-site calculations, thus $Z_u = Z_d = Z$; triangles, circles, boxes: cluster calculations. All lines are just guides to the eye. Inset: the local spectral function projected onto the a_{1g} orbital with V at $x = 3/4$.

tance of non-local correlations [31, 32]. From a 'molecular orbitals' viewpoint, the CDW transition is driven by orbital polarization: the intersite interaction drives the symmetric orbital $|u\rangle$ towards half-filling (hence susceptible to a MIT), while the two asymmetric orbitals $|d_{1,2}\rangle$ are completely filled (with in total $5 = 3(1 + y)$ electrons in each EKL unit cell).

In conclusion, we have shown that several of the intriguing physical properties of layered cobaltates at large x can be explained within a picture of electrons moving in a charge-ordered background. In particular, good quantitative agreement with ARPES spectra has been obtained. Although we have considered a specific realization for the charge-ordered phase in the form of a kagomé structure, we expect similar effects for other ordering patterns in which a large fraction of Co ions localize charge and thus become blocked for electron hopping processes. This blocking makes the system highly sensitive to correlation effects, in particular to intersite Coulomb repulsion. The proximity of a van Hove singularity has also been shown to play a key role. Interesting issues to be addressed in future work are whether such charge blocking can account for the large thermopower observed in this doping regime [33] and whether it can provide a mechanism for the apparent violation of the Luttinger sum rule [9].

[1] M. L. Foo, Y. Wang, S. Watauchi, H. W. Zandbergen, T. He, R. J. Cava, and N. P. Ong, Phys. Rev. Lett. **92**, 247001 (2004).
[2] I. Terasaki, Y. Sasago, and K. Uchinokura, Phys. Rev. B **56**, R12685 (1997).
[3] Q. Huang, M. L. Foo, J. W. Lynn, H. W. Zandbergen, G. Lawes, Y. Wang, B. H. Toby, A. P. Ramirez, N. P. Ong, and R. J. Cava, J. Phys.: Condens. Matter **16**, 5803 (2004).
[4] H. Alloul, I. R. Mukhamedshin, T. A. Platova, and A. V. Dooglav, EPL **85**, 47006 (2009).
[5] K. Takada, H. Sakurai, E. Takayama-Muromachi, F. Izumi, R. A. Dilanian, and T. Sasaki, Nature **422**, 53 (2003).
[6] H. Leligny, D. Grebille, O. Prez, A. Masset, M. Herveieu, C. Michel, and B. Raveau, C. R. Acad. Sci., Paris IIc **2**, 409 (1999).
[7] M. Z. Hasan, Y.-D. Chuang, D. Qian, Y. W. Li, Y. Kong, A. Kuprin, A. V. Fedorov, R. Kimmerling, E. Rotenberg, K. Rossnagel, et al., Phys. Rev. Lett. **92**, 246402 (2004).
[8] T. F. Schulze, M. Brühwiler, P. S. Häfliger, S. M. Kazakov, C. Niedermayer, K. Mattenberger, J. Karpinski, and B. Batlogg, Phys. Rev. B **78**, 205101 (2008).
[9] A. Nicolaou, V. Brouet, M. Zacchigna, I. Vobornik, A. Tejeda, A. Taleb-Ibrahimi, P. Le Fèvre, F. Bertran, S. Hébert, H. Muguerra, et al., Phys. Rev. Lett. **104**, 056403 (2010).
[10] A. Nicolaou, V. Brouet, M. Zacchigna, I. Vobornik, A. Tejeda, A. Taleb-Ibrahimi, P. Le Fvre, F. Bertran, C. Chambon, S. Kubsky, et al., EPL **89**, 37010 (2010).
[11] J. Geck, S. V. Borisenko, H. Berger, H. Eschrig, J. Fink, M. Knupfer, K. Koepernik, A. Koitzsch, A. A. Kordyuk, V. B. Zabolotnyy, et al., Phys. Rev. Lett. **99**, 046403 (2007).
[12] S. Y. Li, L. Taillefer, D. G. Hawthorn, M. A. Tanatar, J. Paglione, M. Sutherland, R. W. Hill, C. H. Wang, and X. H. Chen, Phys. Rev. Lett. **93**, 056401 (2004).
[13] M. Roger, D. J. P. Morris, D. A. Tennant, M. J. Gutmann, J. P. Goff, J. Hoffmann, R. Feyerherm, E. Dudzik, D. Prabhakaran, A. T. Boothroyd, et al., Nature **445**, 631 (2007).
[14] G. J. Shu, A. Prodi, S. Y. Chu, Y. S. Lee, H. S. Sheu, and F. C. Chou, Phys. Rev. B **76**, 184115 (2007).
[15] Y. Hinuma, Y. S. Meng, and G. Ceder, Phys. Rev. B **77**, 224111 (2008).
[16] I. R. Mukhamedshin, H. Alloul, G. Collin, and N. Blanchard, Phys. Rev. Lett. **94**, 247602 (2005).
[17] M.-H. Julien, C. de Vaulx, H. Mayaffre, C. Berthier, M. Horvatić, V. Simonet, J. Wooldridge, G. Balakrishnan, M. R. Lees, D. P. Chen, et al., Phys. Rev. Lett. **100**, 096405 (2008).
[18] G. Lang, J. Bobroff, H. Alloul, G. Collin, and N. Blanchard, Phys. Rev. B **78**, 155116 (2008).
[19] O. I. Motrunich and P. A. Lee, Phys. Rev. B **69**, 214516 (2004).
[20] L. Boehnke and F. Lechermann (2010), arXiv:1012.5943.
[21] C. A. Marianetti and G. Kotliar, Phys. Rev. Lett. **98**,

176405 (2007).

[22] G. Khaliullin and J. Chaloupka, Phys. Rev. B **77**, 104532 (2008).

[23] T. Kroll, A. A. Aligia, and G. A. Sawatzky, Phys. Rev. B **74**, 115124 (2006).

[24] W. Ku, T. Berlijn, and C.-C. Lee, Phys. Rev. Lett. **104**, 216401 (2010).

[25] D. Qian, D. Hsieh, L. Wray, Y.-D. Chuang, A. Fedorov, D. Wu, J. L. Lue, N. L. Wang, L. Viciu, R. J. Cava, et al., Phys. Rev. Lett. **96**, 216405 (2006).

[26] G. Biroli, O. Parcollet, and G. Kotliar, Phys. Rev. B **69**, 205108 (2004).

[27] E. Gull, A. J. Millis, A. I. Lichtenstein, A. N. Rubtsov, M. Troyer, and P. Werner, Rev. Mod. Phys. **83**, 349 (2011).

[28] M. Ferrero, P. S. Cornaglia, L. D. Leo, O. Parcollet, G. Kotliar, and A. Georges, Europhys. Lett. **85**, 57009 (2009).

[29] I. R. Mukhamedshin, H. Alloul, G. Collin, and N. Blanchard, Phys. Rev. Lett. **93**, 167601 (2004).

[30] T. Motohashi, R. Ueda, E. Naujalis, T. Tojo, I. Terasaki, T. Atake, M. Karppinen, and H. Yamauchi, Phys. Rev. B **67**, 064406 (2003).

[31] C. Piefke, L. Boehnke, A. Georges, and F. Lechermann, Phys. Rev. B **82**, 165118 (2010).

[32] H. Li, R. T. Clay, and S. Mazumdar, Phys. Rev. Lett. **106**, 216401 (2011).

[33] K. Haule and G. Kotliar, in *Properties and applications of thermoelectric materials*, edited by V. Zlatic and A. Hewson (Springer, 2009), p. 119, arXiv:0907.0192.